JOURNAL OF MATERIALS SCIENCE 28 (1993) 3398–3408

The effect of S′ phase distribution on the fracture toughness of 8090 alloy

K. D. WOO
Department of Metallurgical Engineering, Chonbuk National University, Chonju, Korea
J. S. CROMPTON
Alcan International Limited, Banbury Laboratory, Banbury, Oxon, UK
J. W. MARTIN
Department of Materials, University of Oxford, Parks Road, Oxford, UK

It has been suggested that one role of the S′ phase in Al–Li–Cu–Mg–Zr alloys is to promote slip homogenization. Heterogeneous slip may decrease fracture toughness by enhancing the nucleation and interlinking of voids in association with grain-boundary phases. S′ phase distribution in 8090 has been varied by (a) applying differing degrees of stretch prior to ageing, (b) applying a low temperature pre-age after solution treatment and stretching, and (c) varying the temperature of final ageing. After each treatment, the dimensions of the intragranular δ′ and S′ phases have been measured, and also that of the intergranular δ phase. The distribution of slip in deformed specimens has also been examined. Tensile and toughness parameters have been measured, and little effect of δ′ and S′ phase sizes on the toughness was detected. The fracture toughness appeared to be sensitive mainly to the yield stress, which in turn was dependent upon the distribution of S′ precipitate. The distribution of S′ precipitate is associated with the degree of prior stretch. It is concluded that, at the ageing temperature studied, the S′ phase particles formed are of dimensions such that they are sheared by dislocations and thus have little slip-homogenizing effect.

1. Introduction

The high strength and fracture toughness of aluminium–lithium (Al–Li) alloys are important factors in their use: these alloys also have a higher stiffness and a lower density than other high-strength aluminium alloys. The high strength in aluminium–lithium alloys is obtained by thermomechanical treatment by the addition of copper, magnesium and zirconium [1, 2].

In 8090, the aluminium, copper and magnesium combine to form S′ (Al_2CuMg) during ageing, which is claimed to improve ductility and fracture toughness through homogenizing slip. If fracture proceeds by the nucleation and interlinking of voids in association with grain-boundary particles, this will be easier the more heterogeneous is the slip [3, 4]. The size, distribution and volume fraction of S′ precipitate have an effect on the slip behaviour, and can be changed by thermomechanical treatment and duplex ageing treatment. These changes of S′ phase have been shown to have an effect on the strength and fatigue properties [5]. If fracture is nucleated at a grain-boundary particle, the toughness of the alloy will be related to the distribution of such particles. Thus grain-boundary fracture by microvoid coalescence will proceed more readily, the more closely spaced the precipitates are in the boundary plane. In a peak aged 8090 alloy, strain localization at the precipitate-free zone (PFZ), and the presence of grain-boundary precipitation have been found to enhance the probability of boundary failure [6].

The purpose of the present investigation was to study the effects of both stretching and duplex ageing treatment with pre-ageing stretch on the toughness, and to correlate these with changes in microstructural features. These features include the S′ phase distribution as well as the δ′ (Al_3Li) phase, the dislocation substructure arising from the stretch, the precipitates at the grain boundary and the formation of a δ′ PFZ.

2. Experimental procedure

The material used in this work was a low copper content 8090 plate manufactured by Alcan International. The composition of this material is shown in Table I. Solution heat treatment was carried out at 545 °C, followed by a cold-water quench. The heat treatments applied are given in Table II. Materials A and B have been used to observe the effect of the degree of stretch, and C and D have been used to observe the effect of the duplex ageing with pre-ageing stretch.

Hardness tests were carried out on a Rockwell hardness tester. The tensile data were obtained from

0022–2461

TABLE I Chemical composition (wt %) of the 8090 alloy

Alloy	Li	Cu	Mg	Zr	Ti	Fe	Si	Al
	2.39	1.18	0.75	0.11	0.05	0.05	0.06	bal.

TABLE II Heat treatments applied to the alloy

Materials	Treatment
A	2% stretched after solution treatment, 10 °C h^{-1} heating rate to 170 °C, 32 h at 170 °C
B	7% stretched after solution treatment, 10 °C h^{-1} heating rate to 170 °C, 32 h at 170 °C
C	7% stretched after solution treatment, 5 days at 95 °C, 10 °C h^{-1} heating rate to 150 °C, 96 h at 150 °C
D	7% stretched after solution treatment, 10 °C h^{-1} heating rate to 150 °C, 96 h at 150 °C

test pieces cut with their gauge length parallel to the longitudinal (L) and the short transverse (S–T) direction.

The measurement of plane strain fracture toughness; K_{1c}, was obtained using a compact tension specimen 26 mm wide and 13 mm thick, in accordance with ASTM E 647–86a. The crack was propagated along the short longitudinal (S–L) direction in air at room temperature. Tensile tests were conducted in air at a constant crosshead speed of 1 mm min^{-1} using an Instron tensile testing machine.

Compression, to observe the deformation behaviour, was carried out as follows: 9.0 mm × 9.0 mm × 9.0 mm specimens were mechanically, then electrolytically polished in a solution containing 25% nitric acid in methanol cooled to − 30 °C at 10 V. The specimens were deformed by an Instron mechanical testing machine along the short (thickness) direction of the specimen. For each alloy, 5% reductions were carried out at room temperature. The surfaces of the deformed specimen were examined optically using a Nikon optical microscope. Thin foils to observe the deformation structures using transmission electron microscopy (TEM) were prepared from a section cut perpendicular to the compressive axes of the specimens. Specimens to observe the grain size were etched in a modified Keller's reagent after the electropolishing described above. Thin foils for TEM work were electrolytically polished using a Fishioni twin-jet polisher in a solution containing 25% nitric acid in methanol cooled to − 30 °C at 15 V. A Philips CM 12 or CM 20 electron microscope was used to examine each foil. It was found that tilting to the ⟨1 0 0⟩ direction provided the best means of obtaining dark-field and bright-field images of δ′ and S′ phases. Dark-field images were obtained by placing the objective aperture over a δ′-superlattice spot or an S′ phase streak to reveal δ′-precipitates and S′ phase rods, respectively.

Lineal roughness parameters for fracture surfaces were measured from optical photographs at × 200. A MOP-AMOS 2 digitizer was used to measure crack lengths. Fractographic studies were carried out using the Hitachi 530 SEM with an accelerating voltage of 25 kV.

3. Results

3.1. The effects of the thermomechanical and the duplex ageing treatments on the microstructure and mechanical properties

In all the materials, optical metallography revealed a predominately unrecrystallized pancake-shaped grain structure with planar grain boundaries lying in the rolling plane. The unrecrystallized structures are attributed to Al_3Zr precipitates inhibiting recrystallization (Fig. 1). A detailed TEM examination was performed to study the microstructure of the alloy. Bright-field imaging revealed the subgrains in the unrecrystallized structures to be approximately 7 μm

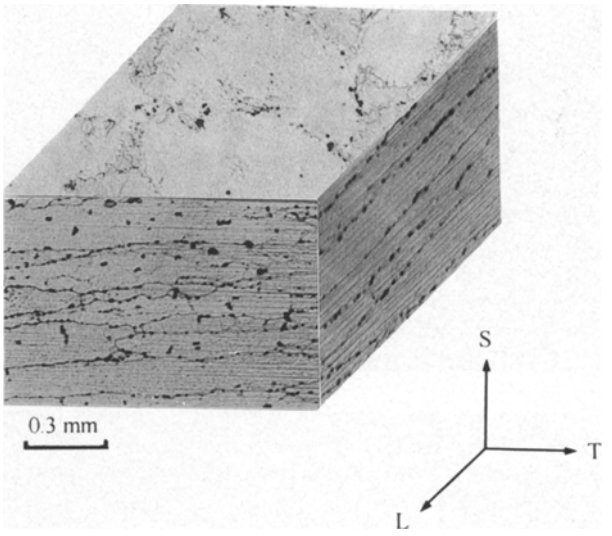

Figure 1 Optical micrograph showing the grain structures of material C.

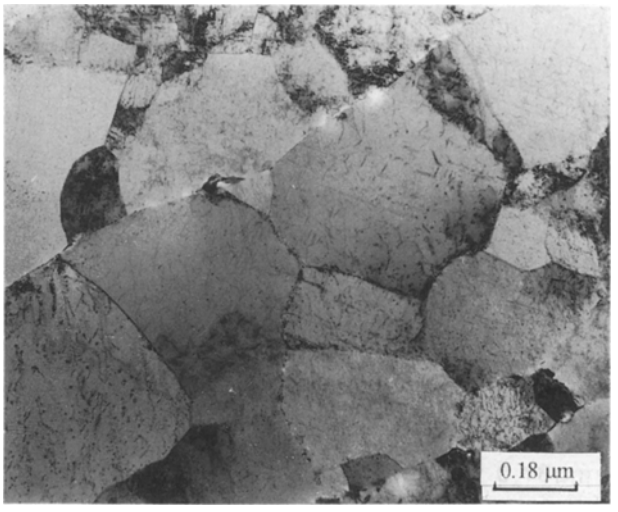

Figure 2 Transmission electron micrograph of material A showing the subgrains in the unrecrystallized structures.

diameter (Fig. 2). Large precipitates were observed at the high-angle grain boundaries.

Fig. 3 shows the distribution of δ′ and S′. The distribution and size of the δ′ and S′ phases were determined by TEM under conditions A, B, C and D (Table III). As shown in Table III, the δ′ precipitates in all the materials were small, spherical and uniform in distribution. The sizes of the δ′ precipitates in materials A and B are larger than those of C and D. These results show that the primary effects on the nucleation and growth kinetics of δ′ precipitates are not from the thermomechanical and the preageing treatment, but are due to the final ageing temperature.

The distribution of S′ precipitates was significantly

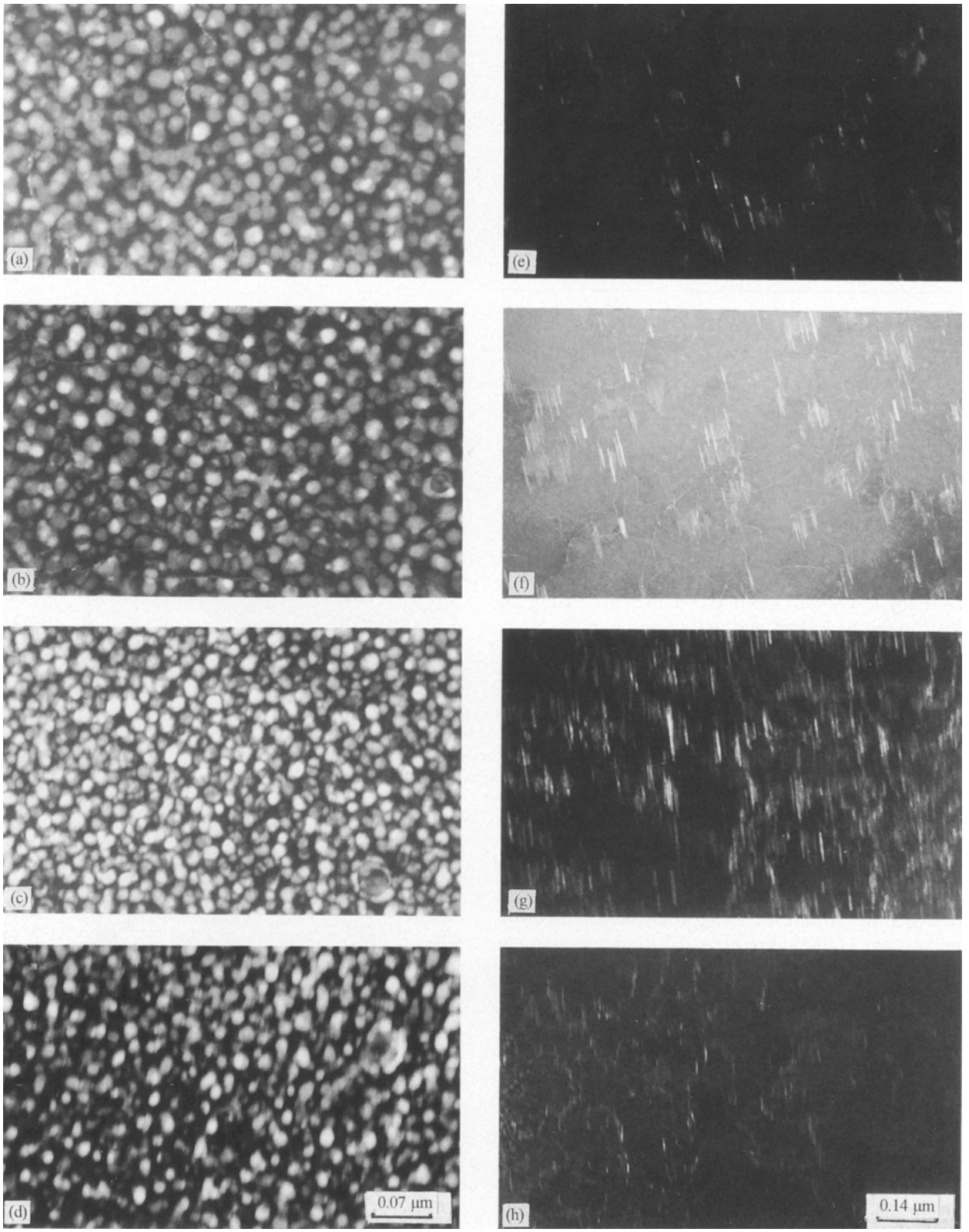

Figure 3 Transmission electron micrographs, $Z = \langle 100 \rangle$, showing distribution of (a–d) δ′ and (e–h) S′ phases in materials (a, e) A, (b, f) B, (c, g) C and (d, h) D.

TABLE III The size of δ′ and S′ phases (± standard deviation)

Materials	δ′ phase	S′ phase	
	Diameter (nm)	Length (nm)	Rod diameter (nm)
A	18.6 ± 1.04	37.86 ± 10.6	3.72 ± 0.46
B	17.2 ± 1.08	51.76 ± 12.8	3.89 ± 0.65
C	12.7 ± 1.07	54.96 ± 13.4	3.29 ± 0.68
D	11.4 ± 1.01	52.49 ± 8.1	2.17 ± 0.53

affected by the thermomechanical and by the duplex ageing treatments. In the 2% stretched material A, the precipitates of S′ were fewer and more inhomogeneous than those of the 7% stretched materials B, C and D. In the 7% stretched and duplex aged material C, the distribution of S′ phase was more homogeneous than that of non-duplex aged material D. The prior stretch followed by the preageing thus had a significant effect on the precipitation of S′. Table III also shows that the size of the S′ precipitates was increased by the greater

TABLE IV Mechanical properties of the materials A, B, C and D

Materials	Yield strength (MPa)	Ultimate tensile strength (MPa)	Elongation (%)	K_{1c} (S–L) (MPa $m^{1/2}$)	Hardness (H_RB)
A	326(S–T)	483	5.5	21.0	75.6
	402(L)	501	7.9		
B	363	502	3.1	16.7	80.5
	460	537	7.7		
C	350	506	5.3	17.0	79.3
	442	530	6.9		
D	335	472	5.0	16.6	80.2
	390	466	7.1		

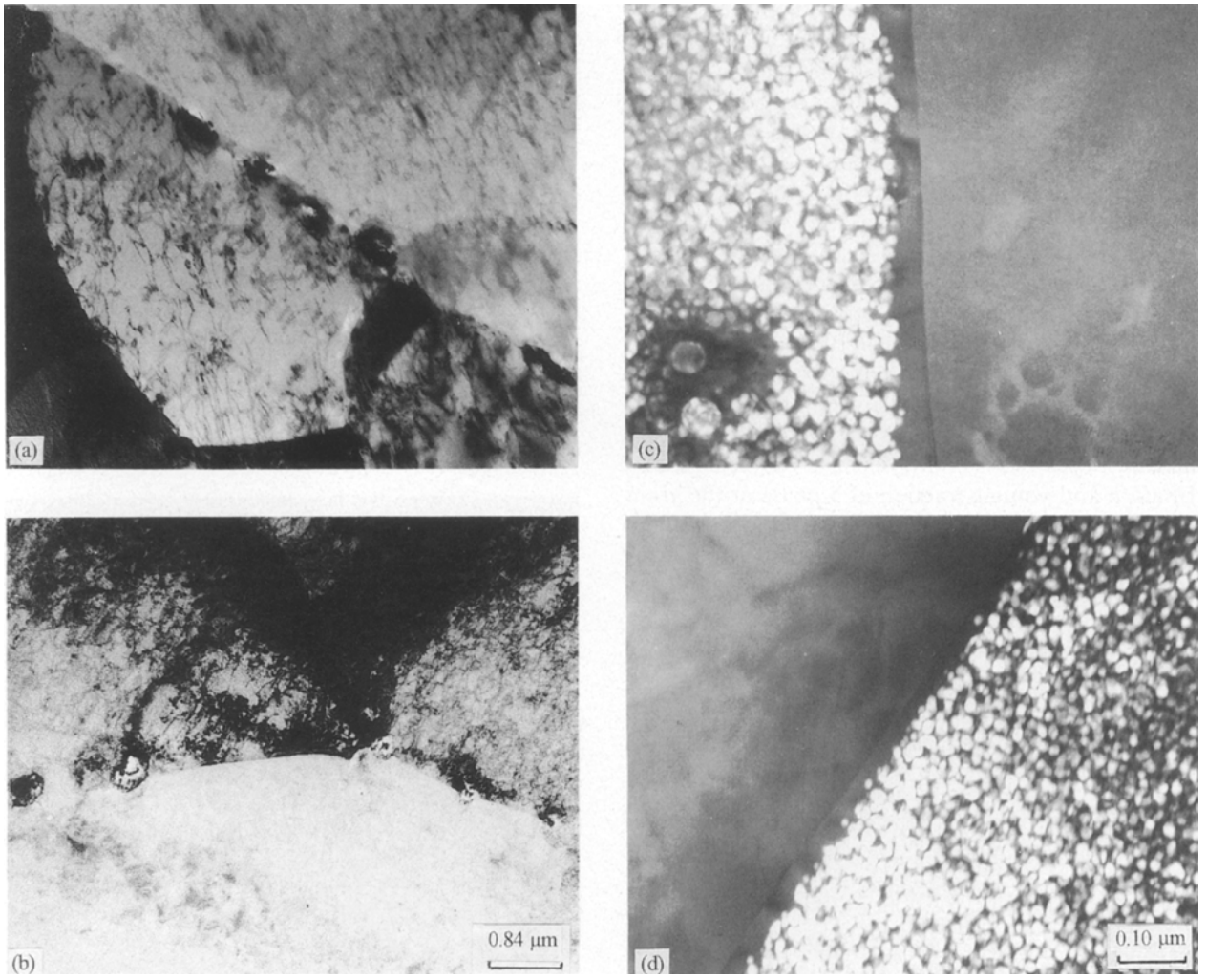

Figure 4 Transmission electron micrographs showing the existence of (a, b) δ and (c, d) δ′-PFZ at the high-angle grain boundaries in materials (a, c) A and (b, d) C.

deformation and by the introduction of the duplex ageing treatment.

Any changes in slip behaviour as a function of the thermo-mechanical and the duplex ageing treatment may be related to the distribution and size of the δ′ and S′ precipitates. The mechanical properties obtained after the various treatments are listed in Table IV. It is seen that the strength increases as the prior deformation increases. The strength of the stretched material with duplex ageing treatment C is higher than that of the stretched material with non-duplex ageing treatment D. The plane strain fracture toughness decreases as the yield strength increases in conditions A and B, but the K_{1c} value of C does not decrease as the yield strength increases, compared with specimen D.

3.2 The effect of the thermomechanical and duplex ageing treatments on grain-boundary precipitation

The effects of the thermomechanical treatment and the duplex ageing treatment combined with stretching on the size of δ phase and width of δ′ PFZ at grain boundaries were observed. δ phase particles were observed at high-angle grain boundaries in materials A and C (Fig. 4). Table V shows that the sizes of δ phase in material B decreased as the degree of deformation increased, but that there were no large differences in the sizes of δ phase between the duplex aged material C and the non-duplex aged material D. The δ particle size was, however, larger at the higher ageing temperature, and this seems to be the primary controlling parameter, rather than the increase of deformation.

There is a difference in the δ′ PFZ width between A and B materials, so we can conclude that stretching has a small influence on this feature. However there is no significant difference of the δ′ PFZ widths between C and D, so duplex ageing treatment with pre-ageing stretch has little effect on the precipitation of δ phase. The δ′ PFZ width increases as the ageing temperature increases, because its width depends on the size, distribution and volume fraction of δ phase at the grain boundary. Thus, one cannot control the width of the δ′ PFZ by increasing the deformation or by the introduction of a duplex ageing treatment.

TABLE V The size of δ phase and the width of δ′ PFZ (± standard deviation)

Materials	Size of δ (nm)		Half PFZ width (nm)
	Length	Width	
A	0.52 ± 0.06	0.37 ± 0.04	40 ± 1.89
B	0.40 ± 0.06	0.33 ± 0.08	34 ± 2.01
C	0.27 ± 0.07	0.23 ± 0.08	25 ± 1.14
D	0.26 ± 0.06	0.22 ± 0.08	22 ± 3.67

In all the materials, S′ PFZs were observed at high-angle grain boundaries, and those in materials A and B are shown in Fig. 5. The measurement of the S′ PFZ width is difficult, because the distribution of S′ phase near the grain boundary is irregular. An S′ PFZ was found at high-angle grain boundaries even if the specimen was 7% stretched, so prior strain does not appear to promote S′ precipitation on high-angle grain boundaries. In contrast, the distribution of S′ precipitate at subgrain boundaries is highly dependent on the degree of deformation (Fig. 6). In material A, the distribution of S′ at the subgrain boundaries is denser than that in the matrix, but there is little difference between the distribution of S′ phase in the matrix and that in the subgrain boundaries in material B, because of the large difference in the dislocation density introduced by the deformation, which dominates the S′-phase nucleation.

3.3. Observations of dislocation distribution

The dislocation configuration of materials A, B and C on the (0 0 1) plane was examined with a dark-field weak-beam technique using a 2 0 0 reflection. As

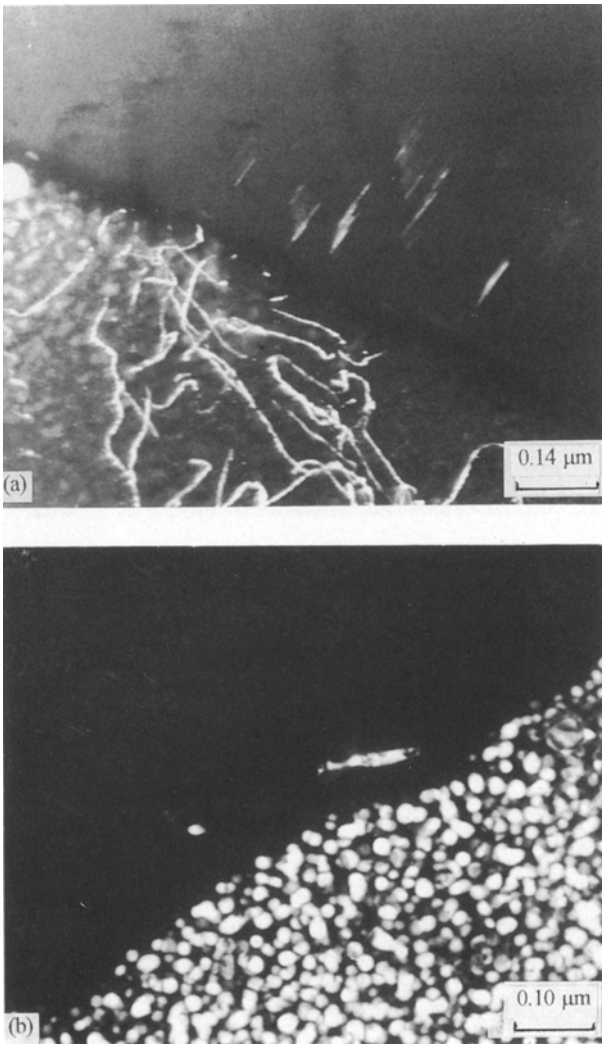

Figure 5 Transmission electron micrographs showing the δ′ PFZ at the high-angle grain boundaries in materials (a) A and (b) B.

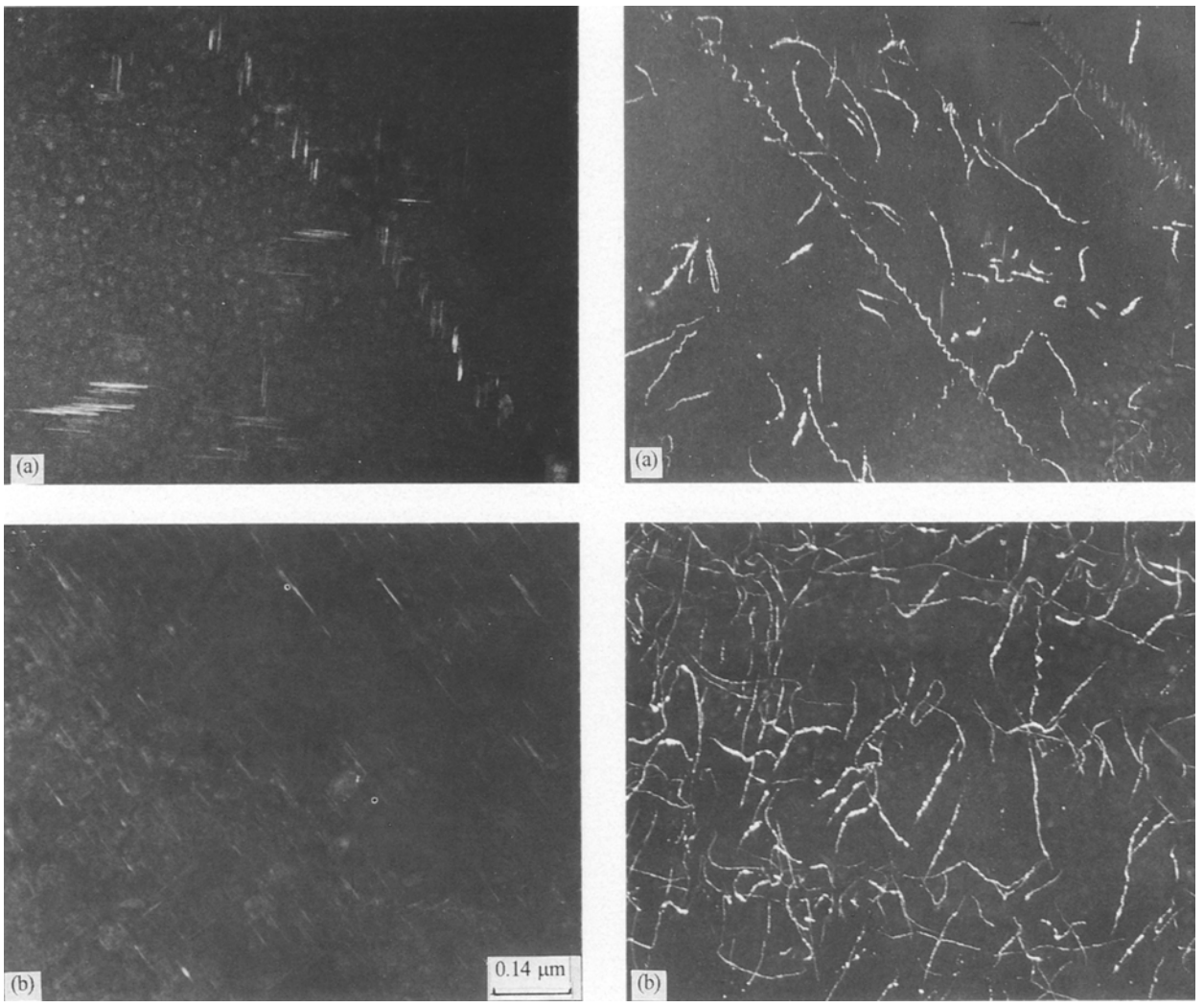

Figure 6 Transmission electron micrographs showing the subgrain-boundary precipitation of S′ phase in materials (a) A and (b) B.

shown in Fig. 7, the dislocations present in all materials are individual dislocations, but no dislocations pairs are present. The dislocation density in materials B and C is higher than that in A.

White spots are observed on the dislocations in all the specimens, which are precipitated S′ phase particles. These will tend to impede the dislocation movement during deformation for fracture, so that a more homogeneous dislocation distribution might be expected after deformation.

3.4 Fractography

Fig. 8 shows the primary cracking at the subgrain boundaries of materials A, B and C. The fracture in these materials was predominantly intergranular. These observations are in agreement with those of Doorbar *et al.* [7]. The fracture surface of these materials show fine dimples on grain-boundary facets. The intergranular fissures at high-angle grain boundaries of materials A and B are shown in Fig. 9 with the crack surface tilted 20 °C to the beam direction. These could be caused by the presence of the δ′ PFZ and the precipitates at the high-angle grain boundaries providing sites for crack nucleation.

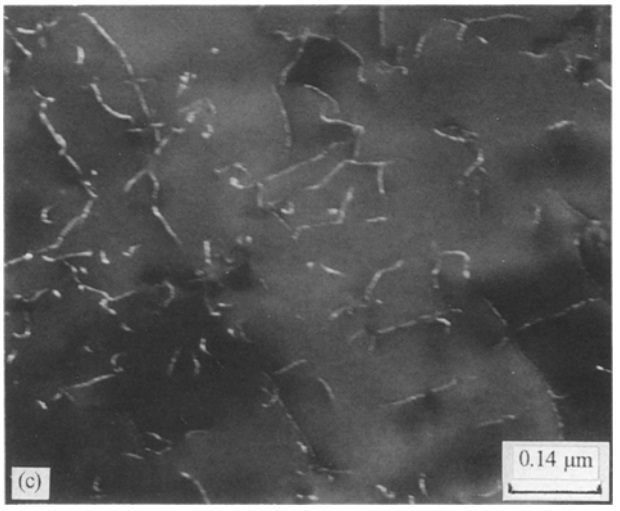

Figure 7 Transmission electron micrographs showing the characteristics of dislocations in the $\mathbf{K}_{1c}$ materials (a) A, (b) B and (c) C.

4. Discussion

4.1. The effects of the thermomechanical treatment and the duplex ageing treatment on the microstructures

The distribution of the S′ phase became more homogeneous at the higher stretch (Fig. 3) due to preferentially nucleation on the dislocations introduced during

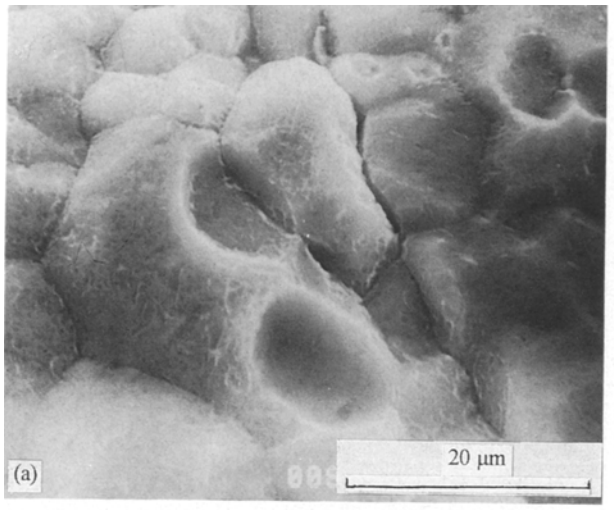

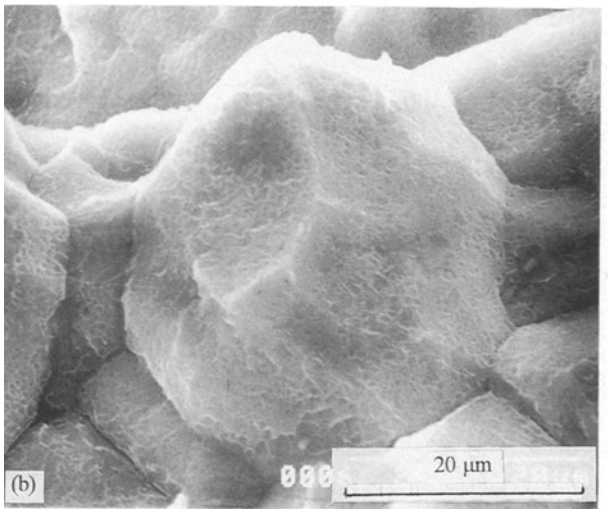

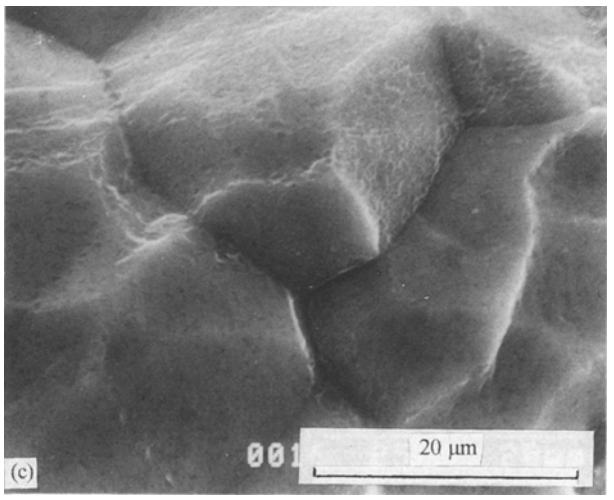

Figure 8 High magnification of scanning electron micrographs of the fracture toughness surfaces (a) A, (b) B and (c) C showing intergranular fracture mode.

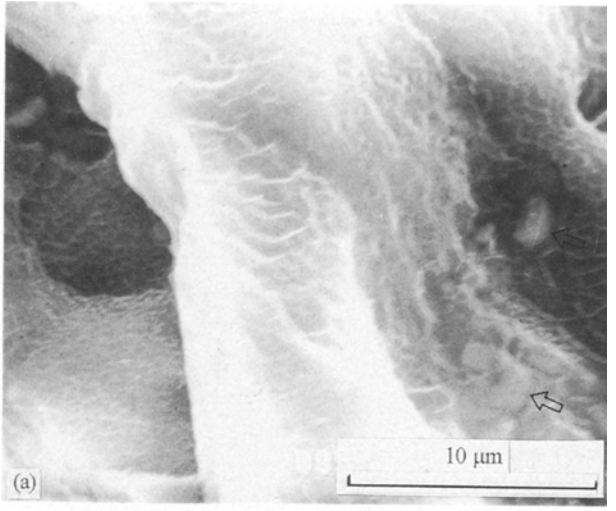

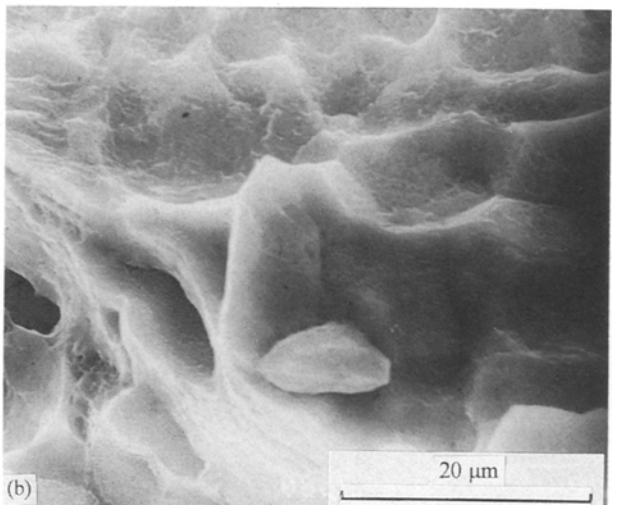

Figure 9 Scanning electron micrographs of materials (a) A and (b) B showing lateral fissure separation between high-angle boundaries.

the stretch, but the δ′ sizes are hardly changed. The effectiveness of the precipitated S′ phases in impeding dislocation motion is greater in the stretched than in the unstretched alloys due to the much more homogeneous distribution and larger size of the S′ particles [5]. Increasing the stretch appears to produce an increased the length of S′ phase because the dislocations also act as pipe diffusion channels for magnesium and copper [8]. The sizes and distributions of δ′ and δ phases is little changed by the greater stretch, but significantly changed by the higher ageing temperature as shown in Tables III and V.

The strength of the duplex-aged material C is higher than that of the non-duplex aged material D, but their toughnesses are almost the same (Table IV). The increased density as well as the more uniform distribution of the S′ precipitate also contributes to the increased strength [9]. The sizes of δ′ and S′ phases in the duplex-aged material C are a little larger than those in D, but the distribution of S′ phase in C is more homogeneous than that in D (Fig. 3 and Table III). The differences in the S′ precipitate distribution are main cause of the difference in the toughness. These results show that the duplex ageing treatment has little effect on the precipitation and growth of δ′ and S′ phases, but has an effect on the distribution of S′ phase. This is because vacancies that had been liberated from the lithium were allowed to coalesce during the pre-ageing treatment, providing nucleation sites for the S′ precipitates [5]. The formation kinetics of S′ phase are accelerated by these effects.

In the case of duplex-aged material which is non-prestretched, even if there are adequate nucleation sites for the S′ phase, the growth of S′ phase is difficult because there are insufficient dislocations to act as pipe-diffusion channels for magnesium and copper [5]. In contrast, the duplex-aged material which is pre-stretched has sufficient dislocations present to act as pipe-diffusion channels, so one would expect the size of S′ phase in C to be affected by not only stretching but also pre-ageing treatment (Table III).

On comparing B and C, the mechanical properties are seen to be almost the same, although the sizes of δ′ and S′ particles, the distribution of S′ particles and the widths of δ′ PFZs are different. This is due to the fact that the distribution of S′ phase in C is more homogeneous than that in B even though the sizes of δ′ and S′ phase in C are smaller than those in B.

4.2. The effect of the size and distribution of δ′ and S′ phases, and slip distribution on the fracture toughness

The size of the δ′ phase is an important factor for controlling the fracture toughness properties. According to Duncan and Martin [10], the materials showing higher toughness correspond to ageing treatments that lead to smaller δ′ precipitate sizes. This, in turn, will result in a less planar slip distribution [11], and hence greater plasticity. In Tables III and IV there is a difference of about 25% in fracture toughness between materials A and B, but the size of the δ′ phase is almost the same. The δ′ size between B and C is quite different by about 40%, but the fracture toughness is the same. This is because the size effect of δ′ phase on the fracture toughness may be swamped by the effects of other precipitates in these materials.

The rod diameter of the S′ precipitates are similar (Table III) in materials A and B, and in the range 3.7–3.9 nm. This diameter is likely to be less than the transition diameter for the transition from particle shearing to Orowan looping, which for a single dislocation has been estimated at 3.1 nm [5]. Because the δ′ phase will tend to promote the formation of planar arrays of dislocations, the critical diameter for shearing the S′ phase is likely to be greater than 3.1 nm. Thus in materials A, B and C, the S′ precipitates will be sheared by dislocations and therefore they will have little slip-homogenizing effect (Figs 10 and 11). There is no significant difference in S′ rod diameter between materials A and B, so the size factor of the S′ phase cannot be the primary reason in these materials for their difference in fracture toughness.

As the slip-band width becomes narrower, the stress concentration at grain boundaries becomes more

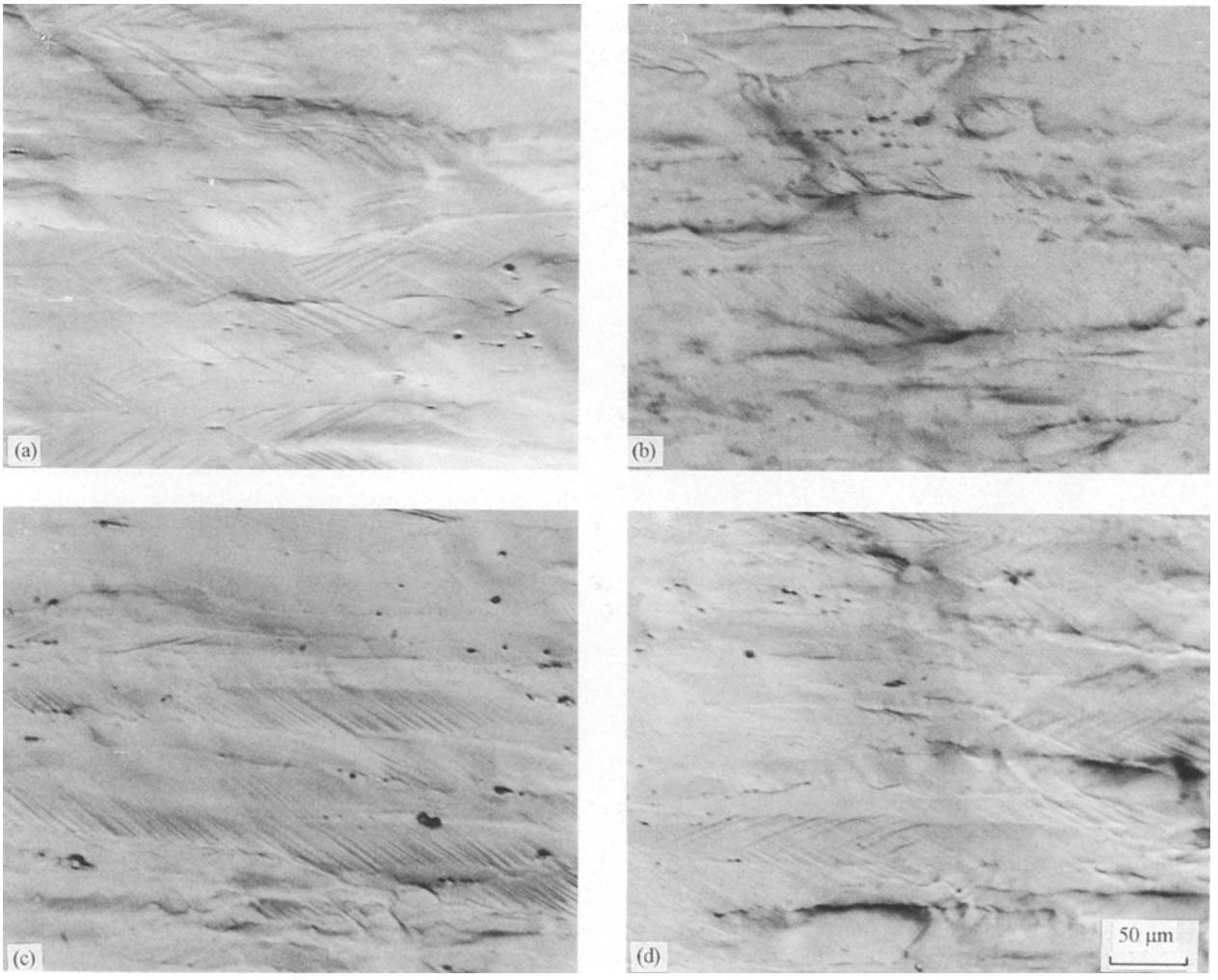

Figure 10 Planar slip in materials (a) A, (b) B, (c) C and (d) D compressed by 5%.

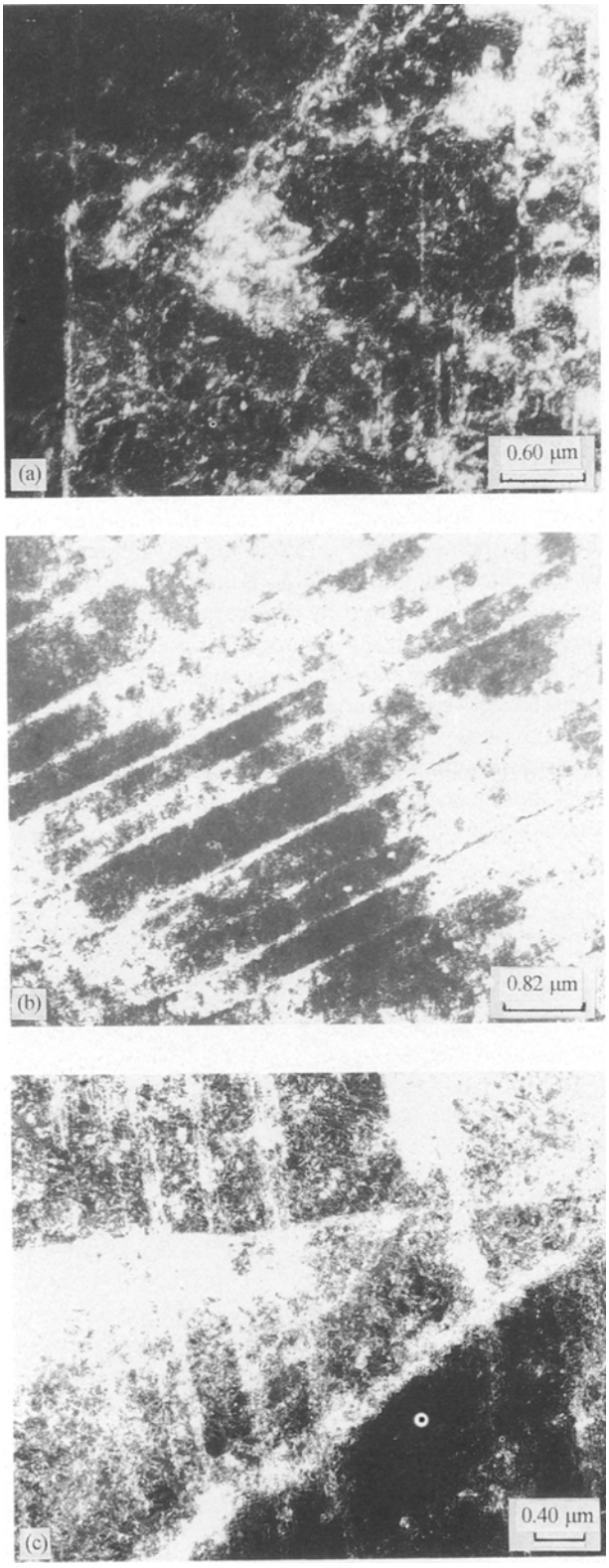

Figure 11 Transmission electron micrographs of materials (a) A, (b) B, and (c) C with ⟨1 1 2⟩ zone axis showing the planar slip bands in 5% compression test materials (g = 2 2 0).

significant, and then the fracture toughness will be decreased [11, 12]. The stress concentration at the grain boundary also becomes more significant as the grain size is increased, but there is no significant difference in grain size between A, B, C and D, because all the materials are the same composition and processing. Fig. 10 shows that the slip lines in all the materials are fine and penetrate through the subgrain boundaries as well as the recrystallized grain boundaries, and the difference in the slip distribution between these materials is not significant. Although well-defined slip lines are observed within the grains, intergranular cracking dominates the fracture behaviour of all the alloys, as noted from the observations of fracture surface topography (Figs 8 and 9). TEM observation was carried out to measure the slip-band spacing and width (Fig. 11). Table VI shows that the slip-band spacings in the K_{1c}-tested materials B are larger than those in the K_{1c}-tested material A, but the slip-band widths in materials B and C are narrower than those in material A. So there is a relationship between slip width and K_{1c} in the materials. The important parameter influencing the fracture toughness is the slip-band width [12, 13]: if the slip-band width decreases, there is a decrease of fracture toughness. In the compression-tested materials (5%), however, there is no significant difference between the materials. The S′ phase distribution is effective upon toughness, but is not significantly effective on slip distribution, as seen in Fig. 10 and Tables IV and VI.

TABLE VI Slip-band spacing and width (± standard deviation)

Materials	Slip band			
	Spacing (μm)		Width (μm)	
	K_{1c} material	Compressed material	K_{1c} material	Compressed material
A	0.40 ± 0.08	0.41 ± 0.09	0.14 ± 0.03	0.06 ± 0.01
B	0.45 ± 0.12	0.55 ± 0.19	0.06 ± 0.01	0.05 ± 0.01
C	0.42 ± 0.09	0.44 ± 0.08	0.08 ± 0.01	0.05 ± 0.02

In these results, the decrease of fracture toughness in materials B may be mainly caused by the fact that the increase in the yield strength due to the homogeneous distribution of S′ phase is accompanied by increasing amounts of strain localization in the slip bands and a concomitant decrease in the strain-hardening exponent and ductility level [13], as shown in Fig. 3. Therefore, increasing the strength due to the homogeneous distribution of S′ phase may cause a decrease in ductility of 8090. These microstructural changes may cause not only intense deformation bands to be formed which accelerate void initiation and coalescence [14], but also may make plastic relaxation at grain-boundary particles more difficult [14, 15].

The amount of slip planarity associated with the growth of small fatigue cracks has been quantified using measurements of the linear roughness parameter, R_L [16]. R_L is the ratio of the actual length of the crack to the length of the crack projected normal to the load. Increasing slip planarity results in a higher value for unstretched and duplex aged materials than that for the stretched materials, further demonstrating that the S′ is relatively ineffective for the homogenizing slip in the unstretched and duplex aged alloys [5].

Table VII shows the values of R_L in the fatigue crack surface and fracture toughness surfaces. R_L of materials A and C is almost same, but their fracture

TABLE VII Fracture surface linear roughness parameters, R_L, of materials A, B and C (± standard deviation)

Materials	R_L		K_{1c} (S–L) (MPa m$^{-1/2}$)
	Fatigue crack surface	Fracture toughness surface	
A	1.20 ± 0.08	1.20 ± 0.09	21.0
B	1.15 ± 0.07	1.17 ± 0.10	16.7
C	1.19 ± 0.09	1.19 ± 0.10	17.0

toughnesses are very different. Therefore, the value of R_L did not exactly correlate with the fracture toughness. This result is good agreement with the results of Gokhalke and Underwood [17].

4.3. Effect of grain-boundary precipitates and PFZ on fracture toughness

In Fig. 4, it is seen that δ phases (a) and a δ′ PFZ (b) are formed at high-angle grain boundaries. The formation of δ at high-angle grain boundaries leads to the concomitant development of a δ′ PFZ. Vasudevan and Doherty [18] have shown that as the area fraction of the grain-boundary precipitate increases, the high concentration of particles leads to poor fracture toughness, irrespective of the degree of planarity of slip.

In Table V, The size of the δ phase and the width of the δ′ PFZ in B, C and D are smaller than those of A, but the fracture toughness of A is higher than those of B, C and D. The δ′ PFZ width between materials B and C is very different, but the fracture toughness is the same. That is, the width of δ′ PFZ in these materials does not affect the fracture toughness. This result may be due to the fact that the area fraction of the grain-boundary precipitates is very low, and these precipitates are only formed at high-angle grain boundaries in these materials. From the results of Lin *et al.* [19], θ″ and θ′ precipitation up to the grain boundaries appears to eliminate the detrimental effects normally associated with δ′ PFZ in similar magnesium-free Al–Cu–Li alloys. But in 8090, δ′ and S′ phases were shown not to be precipitated at high-angle boundaries (Figs 4 and 5), but precipitated in a high density at low-angle grain boundaries (Fig. 6).

The effect of duplex ageing treatment on the precipitation of δ and the formation of a δ′ PFZ is not significant. This is because the pre-ageing temperature is very low, so δ phase is not precipitated by the pre-ageing treatment. This result shows that the effects of the δ′ size and δ′ PFZ width on the fracture toughness are not significant.

4.4. Fractography

All stretched materials show intergranular delamination-type failure along grain boundaries and subgrain boundaries (Figs 8 and 9). The fracture propagated through a number of uncrystallized pancake-grains without significant deviation.

The tendency for grain-boundary failure in these materials has been attributed to planar slip, strain localization in δ′ PFZs, grain-boundary embrittlement as a result of the precipitation of δ, iron-rich and silicon-rich intermetallics [1, 6, 20]. However, the grain boundaries appear to be relatively effective obstacles to deformation due, in part, to the presence of fine recrystallized grains adjoining the unrecrystallized regions and to the intragranular precipitation of S′ which helps to disperse the slip [2, 21]. The fine dimpled substructure on grain-boundary facets in all stretched materials is associated with the formation of microvoids by slip-band impingement at grain boundaries [22] and/or the iron- and silicon-rich constituents, the zirconium dispersoid, the equilibrium δ and T-type ($Al_xCu_yLi_z$) precipitates [23]. The fracture surface of material A is decorated with rod type particles shown as arrow in Fig. 9. These particles appear to be iron- and copper-rich intermetallic compounds, because analysis by EDS revealed a high concentration of iron and copper. Some irregular-type particles mainly consist of silicon and titanium. These coarse second-phase particles are responsible for the nucleation of voids leading to premature cracking and reduced ductility in the Al–Li–Cu–Mg alloy [14]. The presence of coarse particles, either constituent particles aligned in the rolling direction by prior fabrication, or δ particles precipitated during ageing at grain boundaries, which cavitate easily, may not be the primary cause of failure in these materials.

Lateral fissure separation between the high-angle grain boundaries is shown in Fig. 9. This process occurs on two scales, which are microscopically along the secondary crack ledges due to the δ precipitates at high-angle grain boundary [23], and macroscopically between individual grains under the action of the triaxial stress in plane strain, reducing the constraints imposed by the neighbouring grains during plastic deformation and resulting in a reduction in fracture toughness.

The features such as grain-boundary precipitates, δ′ PFZ, and the sizes of δ′ and S′ phases, are not important factors controlling the fracture toughness in all these materials. The main effect on fracture toughness may arise from the change of yield strength which is associated with the homogeneous distribution of S′ precipitate for the given constant volume fraction of δ′ precipitate.

5. Conclusions

1. The decrease in toughness as the strength increases is little affected by the sizes of the grain-boundary precipitates, the PFZ width, or the sizes of δ′ and S′ phases, but is primarily caused by increasing of the yield stress due to the homogeneous distribution of S′ phase arising from the prior stretch.

2. The S′ phase particles formed at the ageing temperature studied are sheared by dislocations and thus have little slip-homogenizing effect.

3. A strength increase without a decrease of fracture toughness is observed after the pre-ageing stretch with a duplex ageing treatment. The pre-ageing stretch

provides the nucleation sites for S′ precipitates and accelerates their growth. Pre-ageing also provides time for the formation of vacancy clusters upon which the S′ can precipitate.

4. The particle sizes of the δ′ formed as a result of both the pre-ageing stretch and the duplex ageing treatment, are only slightly dependent upon the higher deformation and the pre-ageing treatment, but are primarily dependent on the ageing temperature.

5. The formation and growth of the precipitate-free zone and grain-boundary precipitates are not affected by the change of pre-ageing stretch and the introduction of duplex ageing treatment, but are affected by the final ageing temperature.

Acknowledgements

The authors thank Professor Sir Peter Hirsch, FRS, for providing the laboratory facilities and Messrs Alcan International Limited, for providing the alloy. The work has been carried out with the support of the Yonam Foundation in Korea. Dr S. A. Court and Dr G. Mahon are thanked for helpful discussions.

References

1. R. E. CROOKS, PhD dissertation, Georgia Institute of Technology, USA (1982).
2. P. J. GREGSON and H. M. FLOWER, *Acta Metall.* **33** (1985) 527.
3. E. A. STARKE Jr, T. H. SANDERS Jr and I. G. PALMER, *J. Metals* **8** (1981) 24.
4. W. S. MILLER, M. P. THOMAS, D. J. LLOYD and D. CREBER, *Mater. Sci. Tech.* **2** (1986) 1210.
5. D. J. NICHOLLS and J. W. MARTIN, *J. Mater. Sci* **26** (1991) 552.
6. D. DEW-HUGHES, E. CREED and W. S. MILLER, *Mater. Sci. Tech.* **4** (1988) 106.
7. P. J. DOORBAR, J. B. BORRADAILE and D. DRIVER, in "Aluminum–Lithium alloys III" (Conference Proceedings), edited by C. Baker, P. J. Gregson, S. J. Harris and C. J. Peel, (The Institute of Metals, London, 1986) pp. 496–508.
8. X. XIAOXIN and J. W. MARTIN, *J. de Phys.* **48** (1987) 433–38.
9. D. T. MARKEY, R. R. BIEDERMAN and A. J. McCARTHY, in Proceedings of the 3rd International Conference on "Aluminium–Lithium Alloys III", edited by C. Baker, P. J. Gregson, S. J. Harris and C. J. Peel (The Institute of Metals, London, 1986) pp. 173–83.
10. K. J. DUNCAN and J. W. MARTIN, *J. Mater. Sci. Lett*, **10** (1991) 1098.
11. J. M. DUVA, M. A. DAEUBLAER, E. A. STARKE Jr and G. LUETJERING, *Acta Metall*, **36** (1988) 585.
12. J. M. DOWLING and J. W. MARTIN, *ibid.* **24** (1976) 1147.
13. K. J. JATA and E. A. STARKE Jr, *Met. Trans.* **17** (1986) 1011.
14. E. P. BUTLER, N. J. OWEN and D. J. FIELD, *Mater. Sci. Tech.* **1** (1985) 531.
15. T. B. COX and J. R. LOW, *Met. Trans.* **5** (1974) 1457.
16. A. M. GOKHALKE and E. E. UNDERWOOD, *ibid.* **21** (1990) 1193.
17. *Idem*, *ibid.* **21** (1990) 1201.
18. A. K. VASUDEVAN and R. D. DOHERTY, *Acta Metall.* **35** (1987) 1193.
19. F. S. LIN, S. B. CHAKRABORTTY and E. A. STARKE Jr, *Met. Trans.* **13** (1982) 401.
20. S. SURESH, A. K. VASUDEVAN, M. TSTEN and P. R. HOWELL, *Acta Metall.* **35** (1987) 25.
21. C. J. PEEL, B. EVANS, C. A. BAKER, D. A. BENNETT, P. J. GREGSON and H. M. FLOWER, in Proceedings of the 2nd International Conference on "Aluminum-Lithium Alloys II" edited by T. H. Sanders, Jr. and E. A. Starke Jr (The Metallurgical Society of AIME, New York, 1984) pp. 363–92.
22. K. S. SOHN, J. Y. KIM, S. LEE and N. K. KIM, *J. Korean Inst. Met Mater.* **30** (1992) 424.
23. T. S. SRIVATAN and T. ALAN PLACE, *J. Mater. Sci.* **24** (1989) 1543.

Received 1 December
and accepted 8 December 1992